Chapter 5

Experimental transfer of 'coherence': Towards entanglement connection

This chapter is largely based on ref.[37]. Reference[37] refers to the then current literature in 2007 at the time of publication.

5.1 Introduction

The distribution of entanglement between different parties enables the realization of various quantum communication protocols, such as quantum cryptography, dense coding, and teleportation (refs.[3,162], see also chapter 1). Such distribution relies on entanglement swapping, namely the teleportation of entanglement, which aims at entangling two distant systems which never interacted in the past. Important aspects of this striking feature have already been demonstrated with independent sources of entangled light. In the discrete variable regime, one can generate two independent pairs of polarization entangled beams and subject a superposition of two of the beams to a Bell-state analyzer[a]. The two remaining beams are then projected into an entangled state[222]. More recently, unconditional entanglement swapping has been achieved for continuous quantum variables of light[223,224].

However, to enable quantum communication over arbitrary long distances, entanglement needs to be stored in matter systems. In the quantum repeater architecture[9], entanglement is distributed by swapping through a chain of spatially separated entangled pairs of memories, leading to the possibility of scalable long-distance communication (see Fig. 5.1). Connecting entangled matter systems is thus a critical requirement for the practical realization of quantum networks (chapter 1). Along this line, generation of entanglement between atomic systems has been reported, including entanglement of the discrete internal states of two trapped ions[225], long-lived entanglement of macroscopic quantum spins[59] and, heralded entanglement between atomic ensembles in the single excitation regime (refs.[27,34], chapter 3). However, no entanglement

[a]Note that an entanglement swapping scheme with linear optics is inherently probabilistic (with success probability 50%), because it cannot distinguish the two among the four Bell states[222] (except for the case of continuous variable entangled states[223,224]). Strong nonlinearity is physically required to achieve a quantum gate, which allows for distinguishing all four possible Bell-state projections.

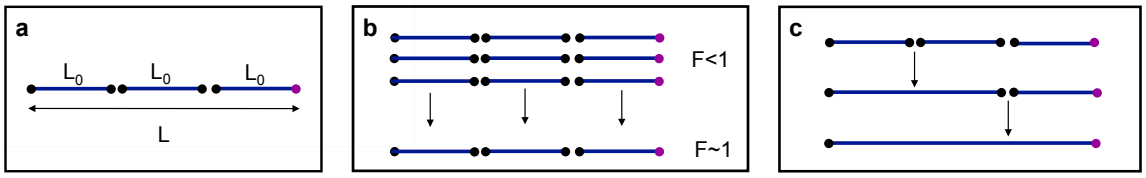

Figure 5.1: **A generic scheme for a bipartite quantum repeater architecture[9]. a**, Entanglement generation and storage. To link two quantum nodes with distance L, we first divide the (long-distance) communication channel into shorter segments (each with length of L_0 and negligible optical attenuation), and generate a linear chain of entangled states in quantum memories (dots). **b**, Entanglement purification. By preparing parallel chains of entangled states in **a**, we probabilistically purify the entangled states with low fidelity $F < 1$ into a single chain comprised of high-fidelity ($F \sim 1$) entangled states. **c**, Entanglement connection. Finally, we sequentially connect the entangled state by entanglement swapping, and eventually prepare a high-fidelity entanglement between the two quantum nodes over a long distance L.

connection has been demonstrated so far with such matter systems. In this chapter, I describe our work towards entanglement connection of atomic ensembles and demonstrate for the first time the transfer of coherence between two atomic ensembles which never interacted[37].

This chapter is organized as follows. In section 5.2, I will give a brief overview of our matter building block, namely an atomic ensemble in the regime of single collective excitation. In section 5.3, I discuss the principles of measurement-induced entanglement between excitation from two remote atomic ensembles, and connection of two pairs. The theoretical model developed in chapter 3 to verify experimentally entanglement is summarized[27,34], and used to give insights into the connection process. The experimental setup is finally presented in section 5.4, together with the experimental results. Finally, I will conclude with our perspectives on realizing entanglement connection experimentally in section 5.5.

5.2 Atomic ensemble in the single-excitation regime

In 2001, Duan, Lukin, Cirac and Zoller (*DLCZ*) proposed an original approach to perform scalable long-distance quantum communications, involving atomic ensembles, linear optics and single photon detectors[4]. The building block is a large ensemble of N identical atoms with a Λ-type level configuration, as shown in Fig. 5.2. A weak light pulse, called write pulse, with frequency close to the $|g\rangle \rightarrow |e\rangle$ transition, illuminates the atoms and induces spontaneous Raman scattering into a photonic mode called field 1. For a low enough write power, such that two excitations are unlikely to occur, the detection of a field 1 photon heralds the storage of a single collective excitation distributed among the whole ensemble. As discussed in chapter 2, the joint state of the atoms and field 1 is a two-mode squeezed state,

$$|\Psi\rangle = |0_a\rangle|0_1\rangle + \sqrt{\chi}|1_a\rangle|1_1\rangle + \mathcal{O}(\chi), \tag{5.1}$$

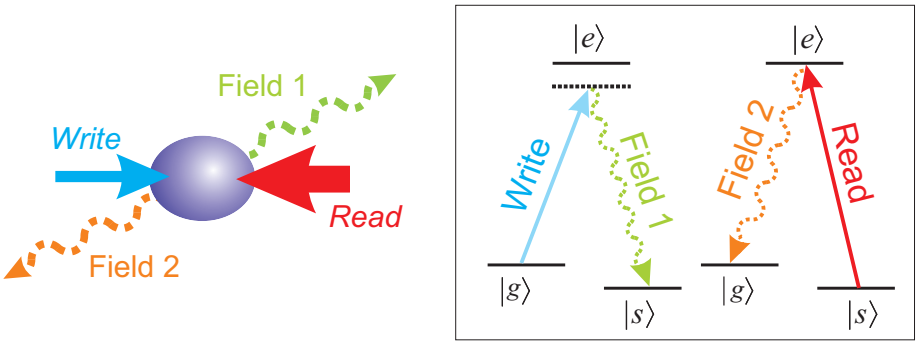

Figure 5.2: ***DLCZ* building block in a counter-propagating and off-axis configuration.** The inset shows the relevant atomic levels for the $6S_{1/2} \rightarrow 6P_{3/2}$ transition in cesium, as well as the associated light fields. The ensemble is initially prepared in $|g\rangle$. A weak write pulse then induces spontaneous Raman transitions $|g\rangle \rightarrow |e\rangle \rightarrow |s\rangle$, resulting with small probability in the emission of a photon (field 1, detected inside a single mode fiber with at a small angle to the write beam) along with the storage of a collective excitation. After a programmable delay, a strong read pulse then maps the state of the atoms to another photonic mode, field 2, via $|s\rangle \rightarrow |e\rangle \rightarrow |g\rangle$.

where $|n_1\rangle$ stands for the state of the field 1 with n photons and χ corresponds to the small probability of a single photon scattered into field 1 by the atoms illuminated by the write pulse. We define $|0_a\rangle \equiv \bigotimes_i^N |g\rangle_i$ and $|1_a\rangle$ denotes a symmetric collective excitation, with

$$|1_a\rangle = \frac{1}{\sqrt{N}} \sum_{i=1}^{N} |g\rangle_1 \cdots |s\rangle_i \cdots |g\rangle_N. \tag{5.2}$$

A read pulse, on resonance with the $|s\rangle \rightarrow |e\rangle$ transition, can later, after a programmable delay, transfer this atomic excitation into another photonic mode, field 2, with collective enhancement (refs. [147,226], chapter 2). After the readout, the resultant state of the fields 1 and 2 is ideally

$$|\Phi\rangle = |0_1\rangle|0_2\rangle + \sqrt{\chi}|1_1\rangle|1_2\rangle + \mathcal{O}(\chi).$$

The two photonic modes, fields 1 and 2, contain quantum correlations [72], precisely as in the case of parametric down-conversion (chapter 2). The lower is the excitation probability $\chi \rightarrow 0$, the better is the approximation of the non-vacuum part by a photon pair, at the price of reduced count rates.

The optically thick atomic ensemble is obtained from cold cesium atoms in a magneto-optical trap (MOT). At a frequency of 40 Hz, the magnetic field is switched off for 7 ms. After waiting about 3 ms for the magnetic field to decay, sequences of writing, reading, and repumping processes are carried out for about 4 ms, with a period of 575 ns. The weak write pulses, with a 200 μm beam waist and linear polarization, are detuned 10 MHz below resonance. The read pulse is orthogonally polarized to the write pulse and mode-matched to it in a counter-propagating configuration. Both write and read pulses are 30 ns long. Fields 1 and 2 are collected into mode-matched fibers with a 3° angle relative to the common direction defined by write and read beams [75], and with a waist of 50 μm defined by the backward projection of our imaging system into the

sample (chapter 2). Before detection, field 1 passes through a filtering stage in order to filter out the photons that are spontaneously emitted when the atoms in the sample go back to $|g\rangle$, without creating the desired collective excitation.

Three parameters well characterize the system experimentally: (i) how well the system is in the single excitation regime, (ii) how efficient is the retrieval of a single excitation, and (iii) how long the excitation can be stored before retrieval while preserving its coherence. The first parameter is determined by a measurement of the suppression of the two-photon component of the field 2 obtained from the retrieval of the excitation[b]. Suppression below 1% of the value for a coherent state has been reported in our system[76]. The ability to efficiently retrieve the excitation is also critical. The probability to have a photon in field 2 in a single spatial mode at the output of the atomic ensemble once an event has been recorded for field 1 can be as high as 50%, leading to a probability around 12.5 % for having a detection event[76]. Last but not least, the writing and retrieval processes can be separated by a programmable delay. As this delay is increased, the above two quantities (two-photon suppression and retrieval efficiency) decay in a typical time scale around 10 to 20 μs. The principal causes for this finite coherence time are the residual magnetic field that inhomogeneously broadens the ground state levels of the atomic samples, as well as the motional decoherence (chapter 2). Detailed theoretical and experimental studies of the decoherence have been reported in refs.[36,78,147,202] (see chapters 3–4).

5.3 Measurement-induced entanglement and connection of atomic ensembles

Starting from this building block, *DLCZ* proposed in their seminal paper to generate and store entanglement for excitation in two remote ensembles and then to connect two pairs. This section presents these measurement-induced schemes, which rely on quantum interference in the detection of a photon emitted by one of the ensembles. After establishing entanglement, directly or via connection, a difficult experimental task is to prove the entanglement[110]. A robust model developed in ref.[27] (see also chapter 3) is then presented.

5.3.1 Entanglement between two ensembles

Let us consider now two atomic ensembles, for which fields 1 are superposed on a $50/50$ beamsplitter, in an indistinguishable way, with the outputs directed towards two single-photon detectors (Fig. 5.3). The detection of a field 1 photon from either of the two ensembles results in an entangled state with one excitation shared coherently between the two ensembles. In more details, after two write pulses are sent into the two ensembles

[b] In chapters 3–4, we have used the parameter $h = \frac{p_{11}}{p_{10}p_{01}}$ to quantify the higher-order excitation for the joint state of the two ensembles. Note that there is analogous parameter, $w = \frac{2p_2}{p_1^2}$ (sometimes, denoted by $g^{(2)}(\tau)$), which quantifies the suppression of higher-order excitation for a single ensemble (or a single beam of light) relative to that of a coherent state ($w = 1$).

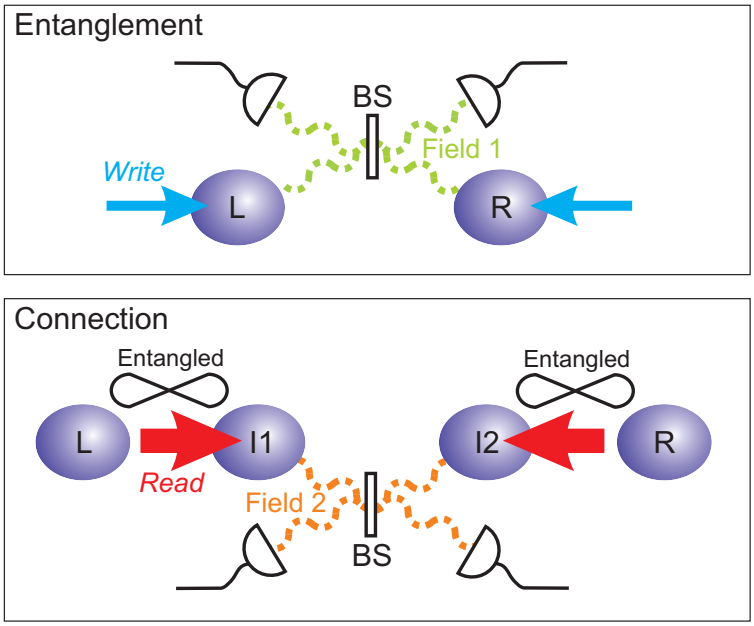

Figure 5.3: **Setups for entanglement generation between two atomic ensembles and entanglement connection between two pairs.** In both cases, the entanglement results from the interference of photonic modes at a 50/50 beamsplitter, with outputs directed towards single-photon detectors. The photonic modes consist in **a**, field 1 modes from both ensembles or **b**, field 2 modes after reading of one ensemble of each pair.

simultaneously, the scattered fields 1 and ensembles are in the product state,

$$\begin{aligned} |\Psi_{LR}\rangle \quad &\propto \quad [|0_a\rangle|0_1\rangle + e^{i\beta_L}\sqrt{\chi}|1_a\rangle|1_1\rangle + \mathcal{O}(\chi)]_L \\ &\otimes[|0_a\rangle|0_1\rangle + e^{i\beta_R}\sqrt{\chi}|1_a\rangle|1_1\rangle + \mathcal{O}(\chi)]_R. \end{aligned} \tag{5.3}$$

Here, β_R and β_L correspond to overall propagation phases determined by the write pulses. Detection of a photon in either detector then projects the state of the ensembles as follows, in the ideal case where higher-order terms are neglected,

$$\begin{aligned} \rho^{'}_{LR} \quad &= \quad \mathrm{Tr}_{1_L 1_R}[\rho(\frac{1}{\sqrt{2}}(a_{1_L} \pm e^{i\theta}a_{1_R})|\Psi_{LR}\rangle)] \\ &= \quad |\Psi^{'}_{LR}\rangle\langle\Psi^{'}_{LR}| \\ \text{with} \quad &\quad |\Psi^{'}_{LR}\rangle = \frac{1}{\sqrt{2}}(|0_a\rangle_L|1_a\rangle_R \pm e^{i\eta}|1_a\rangle_L|0_a\rangle_R). \end{aligned} \tag{5.4}$$

Here, $\rho(|\Psi\rangle) \equiv |\Psi\rangle\langle\Psi|$, $\mathrm{Tr}_{1_L 1_R}$ stands for tracing over the states of fields 1_L and 1_R, a_{1_L} and a_{1_R} are the annihilation operators associated with fields 1_L and 1_R, $\theta = \theta_R - \theta_L$ the difference phase shift between the two field 1 paths from the ensemble to the beamsplitter, and finally the overall phase $\eta = (\beta_L - \beta_R) + (\theta_L - \theta_R)$. This phase η is the sum of the phase difference of the write beams at the L and R ensembles and the phase difference acquired by fields 1 in propagation from the ensembles to the beamsplitter. To achieve entanglement, this phase has to be kept constant (ref. [110], chapter 9). In order to meet this stringent and challenging require-

ment in the initial demonstration reported in[27], the different phases have been independently controlled and actively stabilized by using auxiliary fields. Finally, the $\pm$ sign in Eq. 5.4 comes from the π phase difference between the two outputs of a beamsplitter: depending on which detector records the heralding event, two different entangled states are generated, and stored for subsequent utilization.

5.3.2 Entanglement connection

When two pairs of atomic ensembles are prepared in such an entangled state (Fig. 5.3), one can connect the pairs by sending strong read pulses into one ensemble of each pair. The fields 2 resulting from this readout are then brought to interference at a $50/50$ beamsplitter. Again, a single click on either detector prepares the remaining ensembles in an entangled state[4].

After independent preparation of entanglement for the pairs $\{L, I1\}$ and $\{R, I2\}$ and perfect reading of the states of the ensembles $I1$ and $I2$, the joint state of the fields 2 and the ensembles can be written, neglecting higher-order terms,

$$\begin{aligned} |\Psi_{L,R,2_{I1},2_{I2}}\rangle &= \frac{1}{2}[|0\rangle_{2_{I2}}|1_a\rangle_R \pm e^{i\zeta_{R,I2}}|1\rangle_{2_{I2}}|0_a\rangle_R)] \\ &\quad \otimes[|0\rangle_{2_{I1}}|1_a\rangle_L \pm e^{i\zeta_{L,I1}}|1\rangle_{2_{I1}}|0_a\rangle_L)] \end{aligned} \tag{5.5}$$

where the phases resulting from the entanglement generation and the readout process are given by $\zeta_{i,Ij} = (\beta_{Ij} - \beta_i) + (\theta_{Ij} - \theta_i) + \delta_{Ij}$, with δ_{Ij} the phase of the read beam at the Ij ensemble. Fields 2_{I1} and 2_{I2} are then mixed on a 50/50 beamsplitter, and detection of a photon in either detector projects the remaining two ensembles L and R into

$$\rho_{LR}^{(\pm)} = \mathrm{Tr}_{2_{I1}2_{I2}}[\rho(\frac{1}{\sqrt{2}}(a_{2_{I1}} \pm e^{i\gamma}a_{2_{I2}})|\Psi_{L,R,2_{I1},2_{I2}}\rangle)] \tag{5.6}$$

which can be written as

$$\begin{aligned} \rho_{LR}^{(\pm)} &= \frac{1}{2}|0\rangle\langle 0| + \frac{1}{2}|\Phi_{L,R}^{(\pm)}\rangle\langle\Phi_{L,R}^{(\pm)}| \\ \text{with} \quad & |\Phi_{L,R}^{(\pm)}\rangle = |0\rangle_L|1\rangle_R \pm e^{i\xi}|1\rangle_L|0\rangle_R \end{aligned} \tag{5.7}$$

where $\xi = \zeta_{R,I2} - \zeta_{L,I1} + \gamma$. This overall phase is the sum of the phase difference for entanglement generation for each pair, the phase difference between the two read beams up to the two ensembles and the phase difference of the generated fields 2 from the ensembles to the beamsplitter.

The vacuum part comes from the probability of reading the two excitations at the same time, leaving no remaining excitation in the system. In the ideal case, the connection succeeds 50% of the time. Let us underline also that, significantly, the absolute phases do not necessarily need to be stabilized to succeed in

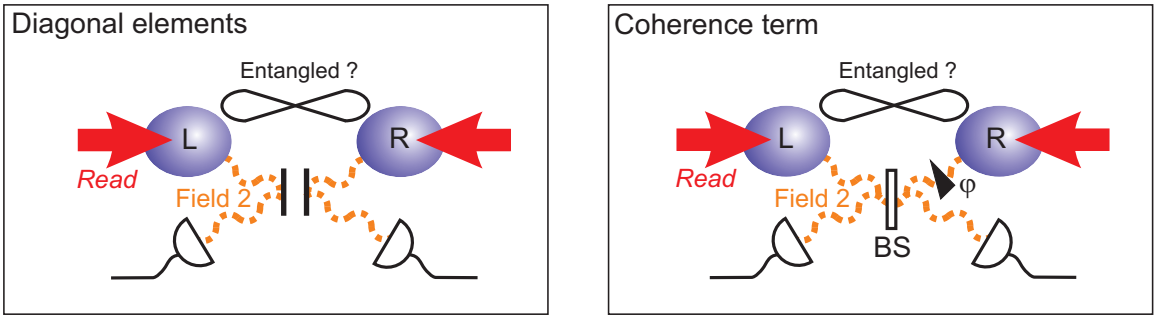

Figure 5.4: **Procedure for verifying entanglement between two atomic ensembles.** The atomic state is mapped to photonic modes via simultaneous strong read pulses and quantum tomography of the generated fields 2 is performed. For this purpose, fields 2 are detected independently (diagonal elements) or in a $50/50$ beamsplitter configuration where the phase of one of the paths is scanned (coherence term).

the connection. Only the overall phase ξ must be kept constant. This feature is exploited in the proposed experimental setup, where passive stability is found to be enough to meet this requirement.

The generated state given by Eq. 5.7 is what *DLCZ* called an "effective maximally-entangled state" (EME) as any state of this form would be purified to a maximally entangled state in the proposed entanglement-based communication scheme[4]. The vacuum coefficient only influences the success probability, but not the overall fidelity of the long-distance communication. This important feature is known as "built-in purification."

5.3.3 Experimental verification of entanglement

To experimentally verify the entanglement between the two atomic ensembles, L and R as sketched in Fig. 5.4, a solution is to map the delocalized atomic excitation into a field state by applying simultaneous strong read pulses. For perfect state transfer, the entangled state of the atoms would be mapped to an ideal entangled state of the two photonic modes (chapter 2).

However, the presence of various noises, the vacuum contribution (coming from a finite retrieval efficiency or also a finite success probability in the case of the swapping), as well as higher-order terms, has to be taken into account. In order to prove experimentally the generation of entanglement at the atomic level, our group has developed in ref.[27] a robust, model-independent determination of entanglement based upon quantum tomography of the fields 2 (chapter 3). As entanglement cannot be increased by local operations on either of the two ensembles, the entanglement for the state of the ensembles will always be greater than or equal to that measured for the light fields. The model consists of reconstructing a reduced density matrix, ρ, obtained from the full density matrix by restricting it to the subspace where no more than one photon populates each mode. It can be shown that this reduced density matrix exhibits less or equal entanglement than does the full one. The model will thus lead to a lower bound of the entanglement, enabling an unambiguous determination of the presence of entanglement, at the price of eventually underestimating its actual magnitude.

The reduced density matrix can be written as

$$\rho = \frac{1}{P}\begin{pmatrix} p_{00} & 0 & 0 & 0 \\ 0 & p_{01} & d & 0 \\ 0 & d^* & p_{10} & 0 \\ 0 & 0 & 0 & p_{11} \end{pmatrix} \tag{5.8}$$

in the photon-number basis $|n\rangle|m\rangle$, with $\{n, m\} = \{0, 1\}$. p_{ij} is the probability of finding i photons in mode 2_L and j in mode 2_R, d is the coherence term between the $|1\rangle|0\rangle$ and $|0\rangle|1\rangle$ states, and $P = p_{00} + p_{01} + p_{10} + p_{11}$. From this density matrix, one can calculate the concurrence C, which is a monotone measurement of entanglement[178]:

$$C = \max(2|d| - 2\sqrt{p_{00}p_{11}}, 0). \tag{5.9}$$

Let us underline, as $d^2 \leq p_{10}p_{01}$, a necessary requirement for $C > 0$ is that there is a suppression of two-photon events relative to the square of the probability of single-photon events for the fields 2, $h \equiv p_{11}/(p_{10}p_{01}) < 1$.

Experimentally, the density matrix is reconstructed by using two different configurations, as sketched in Fig. 5.4. The diagonal elements are determined by measuring individual statistics, i.e., by detecting independently each field. The coherence term can be measured by combining the fields 2 on a $50/50$ beamsplitter and recording the count rate as a function of the phase difference between them. This results in an interference fringe with a visibility V. It can been shown that $d \simeq V(p_{10} + p_{01})/2$. Together, this two-stage measurement gives access to the concurrence C.

5.3.4 Entanglement connection revisited

The principle of entanglement connection has been explained previously in the ideal case where higher-order terms and vacuum contributions are neglected. Let us consider now the more general case, which can be described by the previous approach. We consider two pairs of entangled ensembles and consider that the fields 2 after reading can be described by the same density matrix ρ' with diagonal elements p'_{ij}. The relevant question is now what will be the expression of ρ, the reduced density matrix for the fields 2 of the two remaining ensembles after the connection.

Let us assume that $p'_{10} = p'_{01}$. To later normalize the events conditioned on swapping, one needs to first determine the probability to have a click heralding the connection at one output of the beamsplitter. To the first order, this quantity can be written as

$$p' = 2 \times \frac{1}{2}p'_{10} = p'_{10}. \tag{5.10}$$

The factor $1/2$ corresponds to the 50% chance that the photon be reflected or transmitted at the beamsplitter (i.e., with each detection event uniquely associated with the entangled states $\Phi_{LR}^{(\pm)}$), while the factor 2 results from the symmetry of the scheme where the photon can come from either ensemble.

One can then evaluate, after the reading of the two remaining ensembles, the probability of having one photon for one mode and zero for the other, when a swap event has been detected

$$p_{10} \quad = \quad p_{01} = \frac{1}{2}(p_{10}'^2 + p_{11}' p_{00}' + p_{11}' p_{10}')/p' \sim \frac{1}{2} p_{10}'. \tag{5.11}$$

The terms inside the parenthesis correspond to one photon in mode 2_L and zero in 2_R (or the other way around), and all the other combinations for 2_{I1} and 2_{I2} which can give a swapping event. The final factor $1/2$ comes from the fact, already established before in the ideal case, that the swapping succeeds, to the first order, 50% of the time.

Finally, in a similar way, the probability to have one photon in each mode is given by:

$$p_{11} \quad = \quad \frac{1}{2} p_{11}' (p_{11}' + 2p_{10}')/p' \sim p_{11}'. \tag{5.12}$$

The main feature which appears here is that the weight of the two-photon component stays the same, while the single-photon component is divided by two. As a result, if one calculates for the connected pairs the new suppression h of two-photon events relative to the square of the probability for single-photon events as a function of the initial h' for each entangled pair: $h \sim 4h'$. This result points out the difficulty which could arise in the experimental demonstration of entanglement connection: one needs to start with atomic ensembles entangled with a very low two-photon component, at the price of low count rates and statistics.

5.4 Experimental setup and measurement results

In this section, we present a scheme that permits us to investigate entanglement connection between two pairs of atomic ensembles, without the requirement of any active phase stabilization (see also chapter 4 for a similar setup). Experimental results are finally given.

5.4.1 Experimental setup

The experimental setup is depicted in Fig. 5.5. Two parallel pairs of atomic ensembles are first prepared independently, following the measurement-induced method detailed in section 5.3. This preparation stage is speeded up by real-time conditional control (refs.[36,78], chapter 4): a detection event at either pair triggers intensity modulators that gate off all laser pulses going to the corresponding pair of ensembles, thereby storing the associated state. After successfully preparing both pairs, strong read pulses are sent into the ensembles. The fields 2_{I1} and 2_{I2} are brought to interfere and a detection event on either detector heralds the connection

process. Thanks to the conditional control, a 20-fold enhancement is obtained in the probability to establish the connection (chapter 4), leading to a rate of connection around 4 Hz. Depending on the combinations of field 1 and field 2 detector clicks, two different entangled states $|\Phi_{L,R}^{(\pm)}\rangle$ are generated for the two remaining ensembles, denoted by $+$ and $-$, with a π phase-shift between them.

As pointed out before, the process of connection between the two remaining ensembles, which never interacted in the past, only requires the stability of the relative phase ξ over trials. This overall phase is defined as the phase difference between the absolute phase of all the paths (write beams, field 1, read pulses, and field 2 on the connection side) for the upper pair and the ones for the lower pair. Instead of actively stabilizing all individual phases as it was performed in ref.[27] where two ensembles were involved, this requirement is

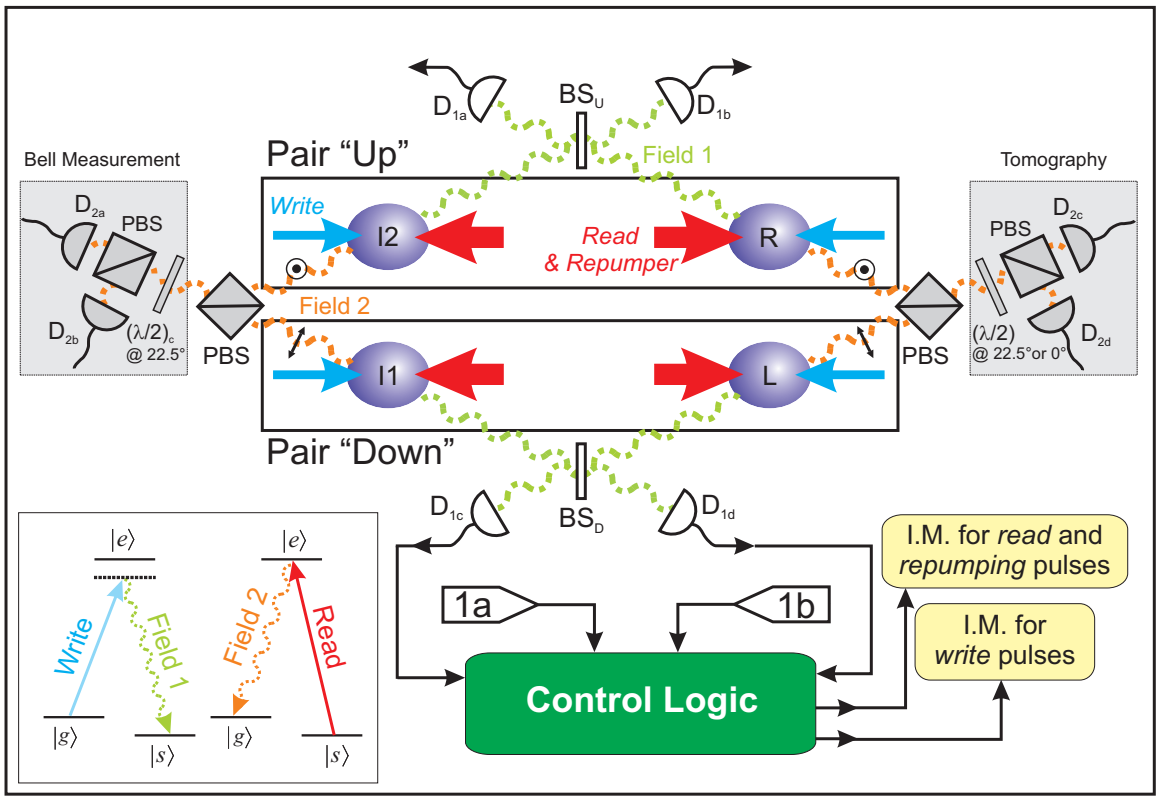

Figure 5.5: **Experimental setup for entanglement connection.** For each pair, "Up" and "Down," the ensembles are separated by 3 meters. Fields 1_{I2} and 1_R from pair "Up" are brought to interference at a 50-50 beamsplitter (BS_U). A photo-detection event at either detector D_{1a} or D_{1b} heralds entanglement between the collective excitation in $I2$ and R. The "Down" pair is prepared in a similar fashion via events at D_{1c}, D_{1d}. A heralding detection event triggers the control logic to gate off the light pulses going to the corresponding ensemble pair by controlling intensity modulators (*IM*). The atomic state is thus stored while waiting for the second ensemble pair to be prepared. After both pairs of ensembles have been prepared, the control logic releases strong read pulses. Fields 2_{I2} and 2_{I1} (2_R and 2_L) are combined with orthogonal polarizations on polarizing beamsplitters. Fields 2_{I2} and 2_{I1} are detected with the half-wave plate $(\lambda/2)_c$ at 22.5°, which is equivalent to a $50/50$ beamsplitter configuration. The fields 2 from the remaining ensembles are characterized conditionally on a detection event heralding the connection. The two configurations of Fig. 5.4 correspond to two different angles, 0° and 22.5°, of the half-wave plate $(\lambda/2)$.

Table 5.1: **Diagonal elements of the density matrix ρ deduced from the records of photoelectric counts, for the two different states after connection, denoted $+$ and $-$.** These values are obtained by considering unit detection efficiency. Errors bars correspond to statistical errors.

Probability	+	-
p_{00}	0.949 ± 0.003	0.948 ± 0.003
p_{10}	$(1.97 \pm 0.05) \times 10^{-2}$	$(1.99 \pm 0.05) \times 10^{-2}$
p_{01}	$(3.06 \pm 0.06) \times 10^{-2}$	$(3.16 \pm 0.06) \times 10^{-2}$
p_{11}	$(4.1 \pm 0.7) \times 10^{-4}$	$(4.9 \pm 0.8) \times 10^{-4}$

fulfilled in our setup by exploiting the passive stability between two independent polarizations propagating in a single interferometer (ref.[36], chapter 4). All the paths for the upper and lower pairs are common, except inside a small interferometer where orthogonal polarizations are separated to define the two ensembles on each side (chapter 3). Operation over more than 24 hours is possible without any adjustment as the phase does not change by more than a few degrees (chapter 3). As a result, no active phase stabilization is required, simplifying significantly the experimental investigation of the connection process. Note that although the present configuration is sufficient to demonstrate the principle of the connection, an experiment where the final pair of ensembles L and R are distant, as in Fig. 5.3b, would require active stabilization of the various phases, since in that case all the paths would be distinct[c]. Our configuration for passive stability is better suited to the case of parallel chains of ensembles, as in the original proposal of *DLCZ*.

5.4.2 Characterization of the states generated upon connection

The generated state is analyzed by using the tomography technique explained in section 5.3.3. Conditioned upon a connection event, the density matrix ρ of the fields 2 is reconstructed following the two required steps: the measurement of the diagonal elements and the determination of the coherence terms.

Table 5.1 gives the measured diagonal elements deduced from the records of photoelectric counts, for both generated states, after a connection event. Unit detection efficiency is assumed, which can only lead to a smaller value for the concurrence than the actual field concurrence for finite detection efficiency. From these values, one can deduce the suppression h of the two-photon events relative to the square of the probability for single-photon events. We find $h_+ = 0.7 \pm 0.1 < 1$ and $h_- = 0.8 \pm 0.1 < 1$. From independent measurements, we inferred the h' parameter for each pair before connection to be $h' = 0.20 \pm 0.05$. The experimentally determined values of h are thus consistent with the expression $h = 4h'$ established previously. As pointed out before, this relation arises from the intrinsic property that the connection succeeds only 50% of the time. This can be seen in the quantities $2p_{01} \sim 4\%$ and $2p_{10} \sim 6\%$, which should be equal to half the retrieval efficiency. The retrieval efficiencies (including detection) independently measured for each ensemble were both around 10%.

In order to access the coherence term, Fig. 5.6 shows the probability of having a detection event on either

[c]The relative phase ζ between the entangled ensembles can in principle be probed, given that ζ is sufficiently stable over the memory time. See section 1.3.1 for more information.

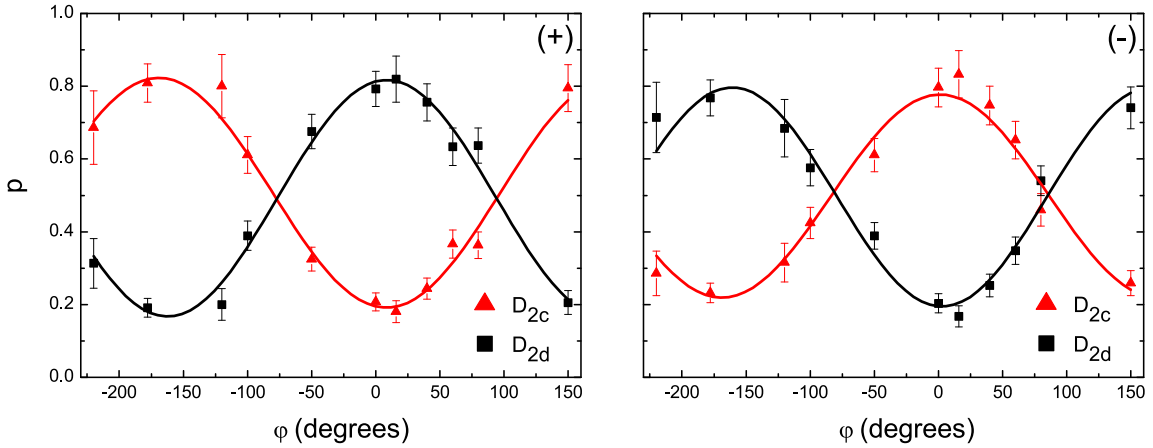

Figure 5.6: **Coherence between the two atomic ensembles L and R induced by the connection event.** p is the probability after connection to have a detection event on either detectors $D2c$ and $D2d$ when the fields 2_L and 2_R interfere, as a function of the phase φ. For each phase setting, data are acquired for 30 minutes, each atomic state being generated overall at about 2 Hz. Errors bars correspond to statistical errors.

output of the beamsplitter, normalized to the sum of these events, as a function of the phase-shift between the fields 2_L and 2_R. Practically, the relative phase is scanned by adjusting the phases of the two classical read beams via birefringent waveplates. The visibilities are found to be $V_+ = 64 \pm 3\%$ and $V_- = 59 \pm 3\%$. A simple model[36] predicts for our excitation probability a visibility equal to $65 \pm 10\%$. By taking into account the measured overlap of the photon wavepacket for fields 2 deduced from a two-photon interference[36], 0.90 ± 0.05, the expected visibility can be roughly estimated to be $55 \pm 10\%$ if all the reduction is attributed to a non-perfect overlap. In the absence of conditioning, the visibility drops to near zero, the residual visibility (below 3%) being explained by finite polarization extinction ratio in our setup. This result demonstrates for the first time the creation of coherence between two atomic ensembles which never interacted in the past. The reconstructed density matrices are shown in Fig. 5.7.

With these data in hand, the concurrences C can be estimated for both states,

$$C_+ = \max\left(-(7 \pm 4) \times 10^{-3}, 0\right) = 0 \tag{5.13}$$

$$C_- = \max\left(-(1.3 \pm 0.4) \times 10^{-2}, 0\right) = 0. \tag{5.14}$$

These values show finally the absence of entanglement, or at least, that our entanglement measurement, which provides a lower bound of the atomic entanglement, cannot detect entanglement in this particular case. One can correct from detection efficiencies and propagation losses[27], but any zero concurrence will stay zero by this correction. The h values confirm anyway that the connected systems are barely in the regime where the two-photon events are suppressed relative to single-photon events. One needs to start with smaller h' for the initial pairs. h' as low as 0.05 can be obtained routinely for each pair in our lab but the count rate to characterize the connection would be prohibitively low.

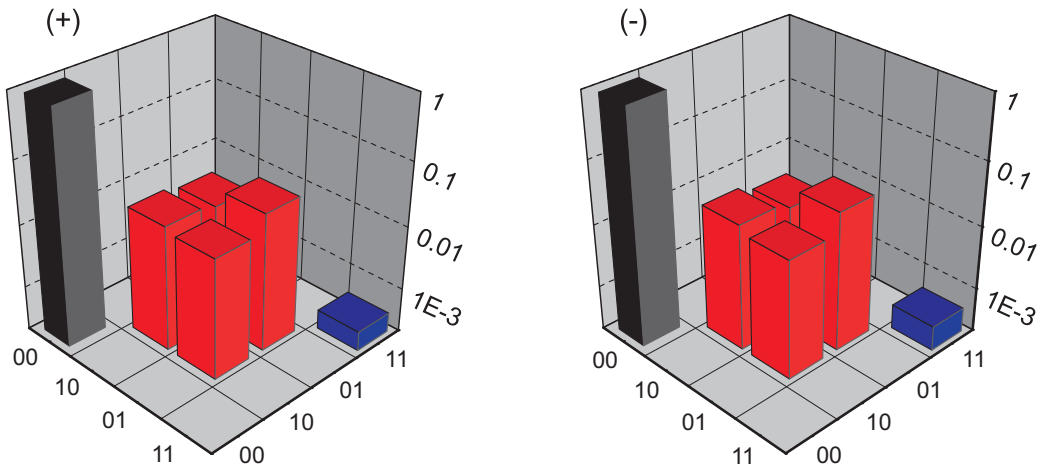

Figure 5.7: **Density matrix for the fields after entanglement connection.** We reconstructed density matrix for both generated states, at the detector location.

5.5 Discussion and prospects towards entanglement connection

In summary, in this chapter, we have presented a possible scheme to demonstrate entanglement connection between atomic ensembles which never interacted in the past. Such striking capability is a critical requirement for the future development of elaborate quantum networks. Our investigation has shown for the first time the creation of coherence upon the connection process. This result validates the proposed setup, in particular its passive phase stability, and constitutes a significant step towards the entanglement connection of matter systems.

To finally generate and prove entanglement connection between the remaining ensembles, very stringent condition on the suppression of the two-photon component needs to be satisfied, at the sacrifice of the count rate in our current setup (chapter 4). Overall, the figure of merit of any elaborate experiment is the product of the probability to prepare the entangled state at each write pulse and the coherence time. Improvements in these two directions have to be explored. The first one can be addressed by, for instance, multiplexing the atomic ensembles. One can imagine to use spatially-resolving detectors, namely array of single-photon detectors, and adaptive optical systems to reconfigure the optical interconnects. Improving the coherence time is a second critical direction as more elaborate protocols are involved. It would require better nulling of the residuals magnetic fields and also the use of improved trapping techniques[147] like a large dipole-trap, as a magneto-optical trap will be rapidly limited by the diffusion of the atoms outside the excitation region (chapter 2). An increase by two orders of magnitude, from tens of μs to ms, would enable, for instance, an experimental demonstration of entanglement connection in our current setup in a few hours of data taking (Fig. 5.8). All together, these improvements would enable deeper investigation of experimental quantum networking, and will definitely lead to fruitful insights into the distribution and processing of quantum information.

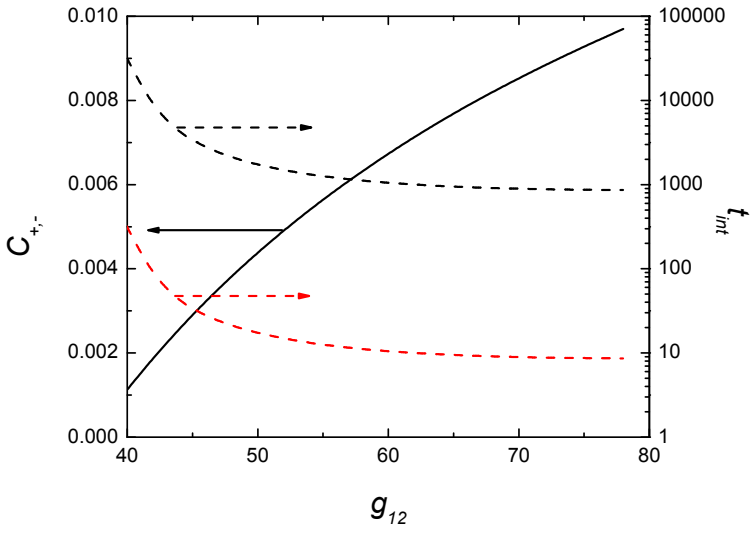

Figure 5.8: **Theoretical concurrence $C_{\pm}$ (black line) after a swapping event as a function of the correlation function g_{12} between fields 1 and 2.** The total integration time to achieve 4 standard deviation statistics for $C_{\pm} > 0$ is given in units of hours with the current memory time of ~ 15 μs (black dashed line) and with the improved coherence time of ~ 1.5 ms (red dashed line).